Dioxygen Activation Kinetics over Distinct Cu Site Types in Cu-CHA Zeolites

Daniel T. Bregante,[1, ¶] Laura N. Wilcox,[2,¶] Changming Liu,[3] Christopher Paolucci,[3] Rajamani Gounder,[2] David W. Flaherty[1,*]

[1]Department of Chemical and Biomolecular Engineering, University of Illinois at Urbana-Champaign, Urbana, IL 61801

[2]Charles D. Davidson School of Chemical Engineering, Purdue University, West Lafayette, IN 47907

[3]Department of Chemical Engineering, University of Virginia, Charlottesville, VA 22904

¶D.T.B. and L.N.W. contributed equally to this work

ABSTRACT: Cu-exchanged zeolites activate dioxygen to form active sites for partial methane oxidation (PMO), nitrogen oxide decomposition, and carbon monoxide oxidation. Apparent rates of O_2 activation depend both on the intrinsic kinetics of distinct Cu site types and the distributions of such sites within a given zeolite, which depend on the density and arrangement of the framework Al atoms. Here, we use hydrothermal synthesis methods to control the arrangement of framework Al sites in chabazite (CHA) zeolites and, in turn, the distinct Cu site types formed. Time-resolved *in situ* resonance Raman spectroscopy reveals the kinetics of O_2 adsorption and activation within these well-defined Cu-CHA materials and the concomitant structural evolution of copper-oxygen (Cu_xO_y) complexes, which are interpreted alongside Cu(I) oxidation kinetics extracted from *in situ* X-ray absorption spectroscopy (XAS). Raman spectra of several plausible Cu_xO_y species simulated using density functional theory suggest that experimental spectra (λ_{ex} = 532 nm) capture the formation of mono(μ-oxo)dicopper species (ZCuOCuZ). Transient experiments show that the timescales required to form Cu_xO_y structures that no longer change in Raman spectra correspond to the durations of oxidative treatments that maximize CH_3OH yields in stoichiometric PMO cycles (approximately 2 h). Yet, these periods extend well beyond the timescales for the complete conversion of the initial Cu(I) intermediates to their Cu(II) states (<0.3 h, reflected in XANES spectra), which demonstrates that Cu_xO_y complexes continue to evolve structurally following rapid oxidation. The dependence of ZCuOCuZ formation rates on O_2 pressure, H_2O pressure, and temperature are consistent with a mechanism in which ZCuOH reduce to form ZCu⁺ sites that bind molecular oxygen and form ZCu-O_2 intermediates. Subsequent reaction with proximate ZCu⁺ form bridging peroxo dicopper complexes that cleave O-O bonds to form ZCuOCuZ in steps facilitated by water. These data and interpretations provide evidence for the chemical processes that link rapid and kinetically irrelevant Cu oxidation steps (frequently probed by XAS and UV-Vis spectroscopy) to the relatively slow genesis of reactive Cu complexes that form CH_3OH during PMO. In doing so, we reveal previously unrecognized complexities in the processes by which Cu ions in zeolites activate O_2 to form active Cu_xO_y complexes, which underscore the insight afforded by judicious combinations of experimental and theoretical techniques.

1.0 INTRODUCTION

Copper ions exchanged onto Al-substituted zeolites facilitate various oxidation reactions and redox cycles, including NO decomposition,[1-2] CO oxidation,[3-4] NO_x (x = 1,2) selective catalytic reduction using NH_3,[5-9] and the partial oxidation of CH_4 to form CH_3OH in stoichiometric[10-17] and catalytic[18-19] cycles. In the context of partial methane oxidation (PMO), Cu(II) ions reduce to their Cu(I) states at high temperatures (e.g., 723 K in He,[14, 17, 20-21] 523 K in 5% CO[20, 22]) prior to exposure to extended O_2 activation treatments (e.g., 723 K, > 2 h) that form active multinuclear Cu(II) species (Cu_xO_y).[14, 21] At lower temperatures, these Cu_xO_y intermediates react readily with CH_4 to form surface methoxy-derived species (e.g., complete consumption within 0.5 h at 473 K), which desorb as CH_3OH upon contact with H_2O in vapor or liquid

phases. The dependence of methanol yields (per Cu) on reaction conditions (e.g., reactant pressure, temperature, time) has been well studied;[11, 14, 17, 23-24] however, comparatively few investigations describe the series of steps responsible for the activation of O_2 molecules or the kinetics and formation of active Cu_xO_y complexes.[11, 22, 24]

Nearly two decades of research have sought to identify the Cu_xO_y species that form upon O_2 activation treatments of Cu-exchanged zeolites and produced numerous proposals (e.g., bis(μ-oxo)dicopper,[1, 10] mono(μ-oxo)dicopper,[11, 13, 16, 22-24] μ-(η^2:η^2)peroxo dicopper,[25] *trans*-η-1,2-peroxo dicopper,[13, 22] bis(μ-hydroxyl)dicopper[26], mono(μ-oxo)tricopper[27-29]). Initial reports from Groothaert *et al.* combined *in situ* extended X-ray absorption fine structure (EXAFS), UV-Vis-near-IR, and electron paramagnetic

resonance (EPR) spectroscopies with comparisons to di-copper metalloenzymes to assign a 22,700 cm^{-1} UV-Vis absorbance feature observed on O_2-activated Cu-ZSM-5 to a bis(μ-oxo)dicopper species.[1, 10] Solomon and coworkers utilized resonance Raman spectroscopy and DFT from which they concluded a bent mono-(μ-oxo)dicopper forms upon O_2 activation over Cu-ZSM-5[11, 23] and Cu-MOR.[24] Recently, van Bokhoven and coworkers examined the formation of PMO active sites in MOR and MAZ zeolites and proposed that proximal [CuOH]$^+$ species form bridged Cu-oxo type species using X-ray powder diffraction, DFT, and XAS.[26, 30-31] Additionally, Pappas *et al.* studied Cu-MOR[13] and Cu-CHA[14] zeolites with varying Cu and Al content and found that O_2 activation requires two Cu centers (i.e., to form mono(μ-oxo)dicopper or *trans*-η-1,2-peroxo dicopper) by using *in situ* X-ray absorption (XAS) and resonance Raman spectroscopies. Lobo and coworkers studied the small-pore zeolite Cu-CHA using Raman spectroscopy to identify vibrational features for *trans*-μ-1,2-peroxo dicopper and mono-(μ-oxo)dicopper, identifying the vibrational features of the latter using ^{18}O-atoms and DFT calculations.[22] In this study, mono-(μ-oxo)dicopper was determined to be the most stable Cu_xO_y site formed as Raman spectra of the O_2-activated sample remained unchanged after four days in O_2 at ambient temperature. In contrast, Lercher and coworkers implicated mono(μ-oxo)tricopper intermediates in both Cu-ZSM-5[28] and Cu-MOR[27, 29] based on Cu-normalized stoichiometric CH_3OH yields (O_2 activation: pure O_2, 723 K, 1 h; CH_4 introduction: 91.2 kPa CH_4 balance He, 473 K, 4 h; CH_3OH extraction: equimolar H_2O and He, 408 K, 0.5 h) that correlated linearly with one-third of the total Cu content, consistent with structures identified within *in situ* EXAFS spectra during O_2 activation. Taken together, this series of contributions presents compelling evidence for multiple and seemingly contradictory conclusions regarding the identity of Cu_xO_y species formed upon O_2 activation over Cu-zeolites, which remains an important area for continued investigation.

The ability of Cu species to bind O_2, cleave the O-O bond, and form distinct Cu_xO_y structures depends strongly upon the spatial and crystallographic distribution of the Al atoms within the zeolite and the fraction of this distribution associated with Cu ions.[20] The Al distribution in a given zeolite depends on its bulk Si/Al ratio and framework topology, and the conditions used for its synthesis, which can collectively lead to significant Cu site heterogeneity among experimental studies. Divalent copper complexes are particularly sensitive to non-uniformities in the arrangement of AlO_4^- sites, because they either require charge compensation from two AlO_4^- centers or coordination to anionic ligands if only one AlO_4^- center is present. As stated by Borfecchia et al., the differences between the many proposals for active Cu_xO_y sites for stoichiometric PMO cycles likely reflect complexities both among the zeolite topologies studied (e.g., ZSM-5, MOR, CHA) and among the varied reaction protocols used (e.g. O_2 activation conditions, CH_4 reaction conditions).[32]

The high symmetry chabazite (CHA) framework provides a model material to study the nature of O_2 activation, because CHA contains a single crystallographically unique tetrahedral site. Moreover, CHA zeolites can be synthesized intentionally with precise control over the relative proximity of framework Al atoms.[33-34] For example, Dusselier and coworkers used this capability to demonstrate on Fe-CHA zeolites that paired Al atoms in the 6-membered ring (MR) (i.e., in second- or third-nearest neighbor configurations) stabilize the PMO active site (α-Fe) and correlate to CH_3OH yields (per Fe) from PMO cycles.[34] Well-defined Cu-CHA materials with controlled speciation of Cu ions can be synthesized wherein 6-MR paired Al sites (2 Al per 6-MR) exchange Cu^{2+} ions (Z_2Cu),[7] while 6-MR isolated framework Al atoms (1 Al per 6-MR) nominally exchange [CuOH]$^+$ species (ZCuOH). Upon O_2 activation of Cu-CHA, a fraction of ZCuOH species form binuclear O_2-bridged structures observed within *in situ* UV-Vis spectra, while Z_2Cu sites do not.[20] These findings agree with reports Z_2Cu sites do not participate in PMO.[14-15, 17] The elementary steps by which O_2 activates over ZCuOH sites to form PMO-active species,[35-36] however, remain elusive.

Here, we use time-resolved *in situ* resonance Raman spectroscopy to measure the spectrokinetics of O_2 activation over well-defined Cu-CHA materials that contain predominantly Cu either at 6-MR isolated or paired Al sites, or mixtures thereof. *In situ* Raman spectroscopy demonstrates that mono(μ-oxo)dicopper complexes form over extended periods (2 – 6 h) similar to those needed to maximize CH_3OH yields, which suggests the Cu_xO_y complexes detected by Raman correspond to the Cu(II) species responsible for PMO. In contrast, *in situ* XAS measurements indicate that Cu(I) converts to Cu(II) intermediates (Cu-O_2; e.g., μ-(η^2:η^2)peroxo dicopper) on much shorter timescales (< 0.3 h), and therefore, the Cu(I) to Cu(II) transformation detected by XAS may signify the formation of a precursor to PMO-active sites. The combination of DFT+*U* computed Raman intensities, steady-state Raman spectra, and ^{18}O-labeling suggest ZCuOH sites activate O_2 to form mono(μ-oxo)dicopper species. Rates of formation for the mono(μ-oxo)dicopper complex are measured as a function of O_2 (5 – 42 kPa O_2) and H_2O pressure (0 – 1 kPa H_2O) and temperature (648 – 773 K) to probe the series of chemical transformations that occur during O_2 activation. These rates depend on the isotopic substitution of water ($k_H/k_D \geq 2$), which suggests that proton transfer may mediate O-O bond cleavage to form mono(μ-oxo)dicopper species. Collectively, these findings provide evidence for the molecular processes that determine the rates at which PMO-active sites form by interactions with O_2 and H_2O reactants.

2.0 MATERIALS AND METHODS

2.1 Raman Spectroscopy

Resonance Raman spectra were obtained on a spectrometer (Renishaw, inVia) equipped with a 532 nm laser. Cu-CHA samples were first pelletized and sieved to retain ~2 mm particles, which were loaded into a temperature-controlled gas-phase reaction cell (Linkam, CCR1000). Cu-CHA samples were first treated to either 723 K in He (Airgas, Ultra-zero grade; 50 cm^3 min^{-1}; 0.33 K s^{-1}) and held for 2 h or to 523 K in 5% CO (Airgas, 99.999%; balance He; 50 cm^3 min^{-1} total flow rate; 0.33 K s^{-1}) for 1 h. After pretreatments in CO, the sample chamber was purged with He (50 cm^3 min^{-1}) for 0.5 h at 523 K. The sample was then heated to a desired temperature in He (0.33 K s^{-1}). Once at the desired O_2-

activation temperature (648 – 773 K), O_2 (Airgas, 99.999%) diluted in He was introduced to the sample to maintain a volumetric flow rate of 50 cm^3 min^{-1} and H_2O (17.8 $M\Omega \cdot cm$) or D_2O (Sigma Aldrich, 99.9% D atom) was introduced using a syringe pump (KD Scientific, Legato 100) through a liquid-injection port. Simultaneously, spectra (0.1 s, 25 co-added spectra) were obtained using line-scan mode with a long 50x objective, such that the power density was approximately 0.4 mW μm^{-2}. All Raman spectra were referenced to the 520 cm^{-1} feature of Si(111). Control experiments which varied the power of the laser (0.04 – 0.8 mW μm^{-2}) and time delays between laser exposure indicate that the measured spectra are not affected by localized heating induced from the laser. In our hands, the CO gas must be purified using a combination of an in-line moisture and O_2 trap (Supelco), as well as Cu turnings (Sigma Aldrich, 99%) that were heated to 553 K. We observed a discoloration of the Cu-CHA surface, which indicates contamination by metal carbonyls, when these traps were not in place. Other contaminants were removed from the O_2 and He streams using inline moisture/hydrocarbon and moisture/hydrocarbon/oxygen combination purifying traps (Supelco), respectively. Consequently, we assume that the partial pressure of H_2O is <10^{-4} Pa (in the absence of intentionally added water vapor), based upon specifications from the gas-trap manufacturers.

The spectral contributions of the independent species formed during O_2 activation of Cu-CHA were obtained by multivariate curve resolution-alternating least squares (MCR-ALS) performed in the WiRE™ software package. Iterative fitting procedures, involving up to five components, were used to describe 99.9% of the data.[37] In all cases, greater than 90% of the variance of the measured spectra was described by a single component, while the other extracted spectra primarily represent changes in the baseline during the course of the experiment related to shifts in the sample position or focus over the course of many hours (Section S8).

2.2 X-Ray Absorption Spectroscopy

X-ray absorption spectroscopy experiments were performed at the Advanced Photon Source (APS), Argonne National Laboratory in Lemont, Illinois, in sector 10 MR-CAT (Materials Research Collaborative Access Team). The insertion device beamline at sector 10 (10-ID) was used for *in situ* experiments. A Cu metal foil reference spectrum (edge energy of 8979 eV) was measured simultaneously with each sample spectrum collected to calibrate the X-ray beam for spectral measurements at the Cu K-edge. All sample spectra were analyzed in WinXAS and normalized using first and third order polynomials for background subtraction of the pre- and post-edges, respectively. The standards used for linear combination fitting (LCF) of the XANES spectra were Cu-CHA dehydrated in 21 kPa O_2 (balance He) at 723 K and Cu_2O (Sigma Aldrich), for Cu(II) and Cu(I), respectively, as shown in Figure S9.

Auto-reduction in inert helium (99.999% UHP), flowed through an oxygen/moisture trap (Matheson, MTRP-0019-XX) at a flow rate of 50 cm^3 min^{-1}, was studied at 723 K (0.167 K s^{-1}) until the XANES spectra stopped changing (sample dependent, up to 2 h). For the oxidation treatment, the sample was held in oxygen (21 kPa in balance He) at a total flow of 50 cm^3 min^{-1} while increasing the temperature from ambient to 723 K (0.167 K s^{-1}) and holding at temperature for up to 2 h.

2.3 Partial Methane Oxidation

Cu-CHA samples were first pretreated in He (UHP, Indiana Oxygen, 50 cm^3 min^{-1}) at 723 K (0.167 K s^{-1}) for 2 h followed by activation in dry air (21 kPa O_2, Zero grade air, 50 cm^3 min^{-1}) at 723 K for various times (0 – 15 ks) and then cooled to ambient temperature in He (Indiana Oxygen, 99.999%, 50 cm^3 min^{-1}). Methane (20 kPa, Indiana Oxygen, 99.999%) with balance of helium (81 kPa) was introduced and heated to reaction temperature of 473 K at 0.167 K s^{-1} and held for 0.5 h. Prior to methanol extraction, the system was purged with He (0.1 h, 50 cm^3 min^{-1}) and then the flow was switched to 2.5 kPa H_2O in a He carrier (30 cm^3 min^{-1}) at 473 K for 1 h. An online mass selective detector (Agilent, 5973N) was used to quantify methanol (m/z^+ = 31) using Ar (Indiana Oxygen, 99.999%) as a calibration standard (m/z^+ = 40), and to monitor potential side products including CO, CO_2, CH_2O, and C_2H_6O (m/z^+ = 28, 44, 29, 45, respectively).

2.4 Density Functional Theory Calculations

Calculations were performed using the Vienna ab initio Simulation Package (VASP)[38] version 5.4.4. For all calculations, only considered the Γ point was considered when sampling the first Brillouin zone. Periodic spin-polarized DFT+U calculations were performed with a 400 eV cutoff energy, a plane-wave basis, and the PBE functional coupled with a semi-empirical D3 dispersion correction with Becke–Johnson damping[39-40] on a CHA supercell containing 12 T-sites. Electron-ion interactions were described with projector augmented wave (PAW)[41] method. For the +U calculations, the U value for the d-orbitals of Cu was set to 6.0 eV based on a recent benchmarking study by Chen et al.[42] Lowest energy Cu dimer structures were sampled over 150 ps 300 K ab initio molecular dynamics (AIMD) simulations with NVT ensemble with Nosé–Hoover thermostat.[20] Unique local minima for each Cu dimer motif were identified by optimizing 400 structures (equally spaced in time). The structures were relaxed until all forces were smaller than 0.01 eV/Å, with a convergence criterion of 10^{-8} eV for energies inside self-consistent-field (SCF) cycles. Raman intensity calculations followed the same protocol described by Liang et al.[43] For Cu dimer structures with multiple unique local minima, spectra were Boltzmann-averaged to compute the final spectra reported in Figures 3 and S15:

$$\langle I \rangle = \frac{\sum_i I_i e^{-E_i/k_B T}}{\sum_i e^{-E_i/k_B T}} \tag{1}$$

where $\langle I \rangle$ is the Boltzmann averaged Raman intensity for a Cu dimer type (e.g., IV), I_i is the simulated spectra of the ith
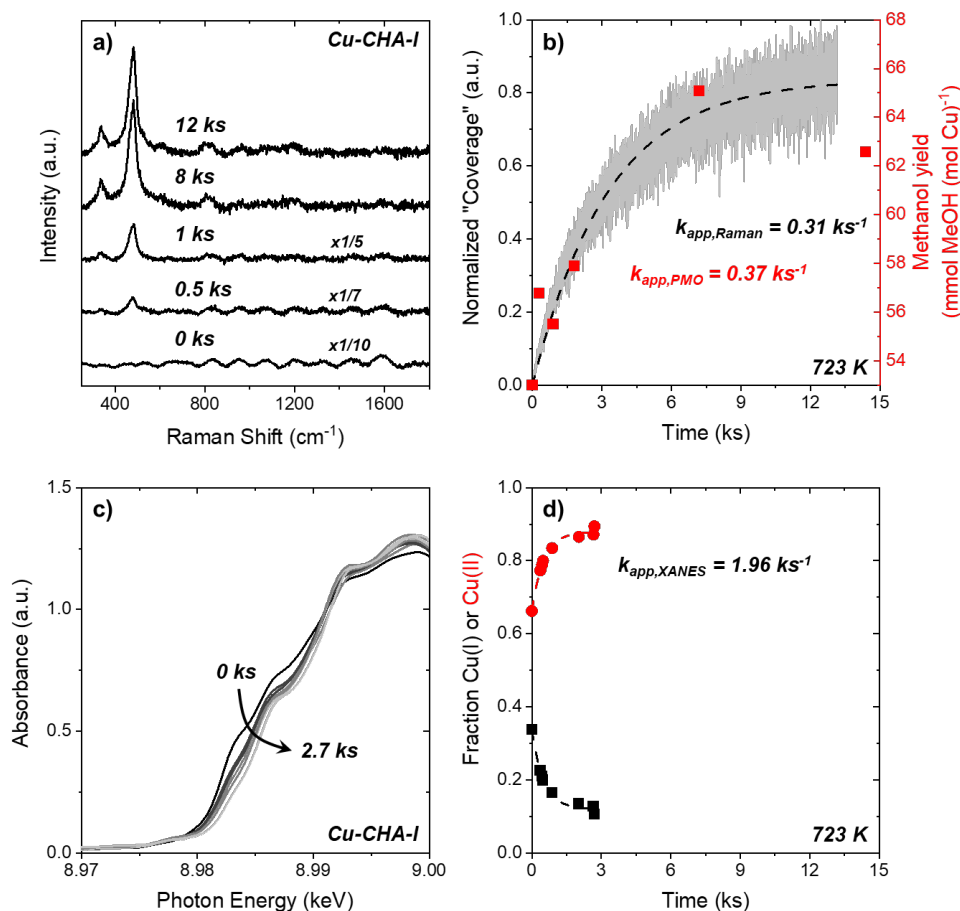
Figure 1. Time-resolved resonance Raman (λ_{ex} = 532 nm) and X-ray absorption spectra of Cu-CHA-I during activation within O_2 (21 kPa O_2, 80 kPa He, 723 K). a) Selected Raman spectra of Cu-CHA-I at periodic intervals after introduction of O_2, and b) the normalized contribution (i.e., coverage) of the steady-state Raman spectrum obtained through MCR-ALS (gray line, −) together with corresponding methanol yields normalized by the Cu content (red ■) for the Cu-CHA-I sample. c) X-ray absorption spectra of Cu-CHA-I obtained after introduction of O_2, and d) the corresponding fraction of Cu(I) (black ■) and Cu(II) (red ●) as a function of time (see Section S5 for fitting procedure). Cu-CHA-I samples were reduced in He at 723 K for 2 h prior to the introduction of O_2. All spectra in panel a) are vertically offset and scaled by the indicated amount for clarity. The dashed curves in panels b) and d) represent fits to a first-order rate expression to the Raman-derived coverages and XANES-derived Cu fractions, respectively.

local minimum within that dimer type (e.g., IV-1), k_B is the Boltzmann constant, E_i is the energy spectra of the ith local minimum within that type, and T is the temperature. Figure S15 reports the computed spectra for each Cu dimer and local minima. All unique local minima structures used to compute frequencies are provided in the SI, Section S7.

3.0 RESULTS AND DISCUSSION
3.1 Disparate Timescales for Cu Oxidation and Cu_xO_y Formation Observed via X-ray Absorption and Raman Spectroscopy

The thermodynamics of copper oxidation and reduction depends on Cu site speciation, and in turn, the zeolite composition and framework Al arrangement, as shown by the DFT-derived phase diagrams reported by Paolucci *et al.*[7] All Cu ions at 6-MR paired sites are in their Cu(II) states at 723 K (21 kPa O_2), while Cu ions at 6-MR isolated Al sites may reside as mixtures of Cu(II) and Cu(I) states at 723 K (21 kPa O_2). The Cu speciation also influences observed auto-reduction behavior at 673 K (1 Pa O_2 in balance He), as Z_2Cu sites remain Cu(II) while ZCuOH sites

thermodynamically prefer the Cu(I) state.[14] Elementary steps to complete ZCuOH auto-reduction events likely require two [CuOH]+ within close enough proximity to form binuclear Cu-oxo species,[44] which suggests that spatially distant ZCuOH sites will not auto-reduce.[14] This interpretation is consistent with Raman spectra (λ_{ex} = 532 nm, 18,800 cm^{-1}) collected in He at 723 K that do not show discernible features for binuclear Cu-oxo structures, (Figure 1a; spectrum at 0 ks solely reflects background fluorescence), which if formed presumably have auto-reduced.

The Cu-CHA samples studied here will be referred to as Cu-CHA-I, Cu-CHA-P or Cu-CHA-M where I, P, and M contain Cu exchanged at predominantly 6-MR isolated Al sites, 6-MR paired Al sites, or mixtures thereof, respectively. All Cu-CHA samples exhibit UV-Vis absorption features between 8,000 and 20,000 cm^{-1} after O_2 activation at 723 K (Figures S3 – S5), which are consistent with the Cu speciation expected within Cu-CHA materials that contain predominantly ZCuOH sites, Z_2Cu, or mixtures thereof.[20]

Figure 1a shows *in situ* resonance Raman spectra of Cu-CHA-I during O_2 activation, demonstrating that more than 7

ks (~2 h) at 723 K is required for Cu_xO_y to reach their steady-state structures. These spectra were obtained with an excitation wavelength of 532 nm to achieve resonance Raman spectra. To capture the transient changes in the number of Raman-active species, we continuously collect Raman spectra during O_2 activation. Multivariate curve resolution-alternating least squares (MCR-ALS) analysis allows us to recover the changes in spectral contributions over time from each kinetically and spectroscopically distinguishable species.[37, 45] For each sample, we find that a single component (i.e., spectrum) and concentration profile describes the time-resolved measurements. If two or more components are modeled, the additional spectra resemble changes within the spectral baseline or random fluctuations in the measurements (See Section S8) and do not contain features consistent with reported Cu_xO_y complexes (*vide infra*) or the CHA framework.

During O_2 activation treatments at 723 K (21 kPa O_2, 80 kPa He), the formation of Raman-active Cu_xO_y species occurs over a period of 12 ks (Figure 1b), while the near-complete oxidation of Cu(I) to Cu(II) approaches a steady-state within 1 ks as monitored by X-ray absorption near edge spectroscopy (XANES; Figure 1d). In both cases, the rate (r_{app}) of O_2 activation (Raman) and Cu(I) oxidation (XANES) follows pseudo-first order kinetics:

$$r_{app} = k_{app}[Cu(I)] \tag{2}$$

where k_{app} is the apparent rate constant and [Cu(I)] is the molar density of Cu(I) ions in the Cu-CHA sample. Within Cu-CHA-I, the rate constant for Cu(I) oxidation ($k_{app,XANES}$ = 1.96 ks^{-1}) is 6-times greater than the rate constant to form the Cu_xO_y species observed by Raman spectroscopy ($k_{app,Raman}$ = 0.31 ks^{-1}). Similarly, the rate constants for Cu(I) oxidation within Cu-CHA-M (Figure S14; $k_{app,XANES}$ = 4.01 ks^{-1}) are 40-fold greater than rate constant obtained from transients measured by Raman ($k_{app,Raman}$ = 0.10 ks^{-1}). *In situ* EXAFS after 1 ks reveal that Cu sites in Cu-CHA-M (Table S6) and Cu-CHA-I (Table S4) are three-coordinate. These spectral features are distinct from those observed in Raman (Figure 2) and EXAFS (four-coordinate Cu; Table S5) of Cu-CHA-P that contain predominantly Cu(II) before and after contact with O_2 (Figure S11) as expected for Z_2Cu sites that are PMO-inactive.

Importantly, the yields of CH_3OH (per mol of Cu) increase monotonically from 0 to ~10 ks over Cu-CHA-I (Figure 1b), and k_{app} values measured via Raman (0.31 ks^{-1}) and PMO (0.37 ks^{-1}) are in close agreement, suggesting that the features within these Raman spectra reflect PMO-relevant active sites proposed previously to be binuclear Cu-oxo site types that require longer timescales to form.[14, 16, 18, 22] A non-negligible amount of methanol forms on Cu-CHA-I following a pretreatment in helium (Figure 1b; zero O_2 activation time) followed by exposure to methane. The formation of methanol without an intentional oxidative treatment was also observed by Pappas et al. on Cu-CHA and ascribed to a small fraction of Cu remaining as Cu(II) in multinuclear Cu_xO_y structures that do not auto-reduce and are thus able to activate methane.[14] Brezicki et al. reported similar findings for Cu-MOR and instead attributed this to trace oxygen impurities in the sample or reaction apparatus.[17] We cannot exclude the possibility that minority Cu_xO_y species are present that do not auto-reduce and subsequently activate methane, or the possibility of trace oxygen impurities as the reason for non-zero methanol yields observed without intentional oxidative treatments. We can, however, definitively conclude that methanol yields increase with longer O_2 activation times (>2 h) due to the formation of the Cu_xO_y structure probed via Raman spectroscopy.

These comparisons demonstrate three critical points with broad significance for stoichiometric and catalytic oxidation reactions performed over Cu exchanged zeolites. First, Cu ions oxidize quickly to form Cu(II) and the majority of Cu exists as Cu(II) within 2 ks. Consequently, the Cu_xO_y species responsible for the Raman scattering features (Figure 1a) must correspond to a Cu(II) complex. Second, changes observed by Raman over longer timescales suggest that following a rapid oxidation of Cu(I) to Cu(II) the structure of the Cu complexes continue to evolve through subsequent processes that occur at slower rates to form the Raman active Cu_xO_y species. Third, yields of CH_3OH formed by PMO continue to increase well after the Cu(I) to Cu(II) transition period and correlate strongly with the numbers of the Raman-resonant Cu_xO_y complexes, which suggests this Cu_xO_y species are linked to the active intermediates responsible for partial methane oxidation.

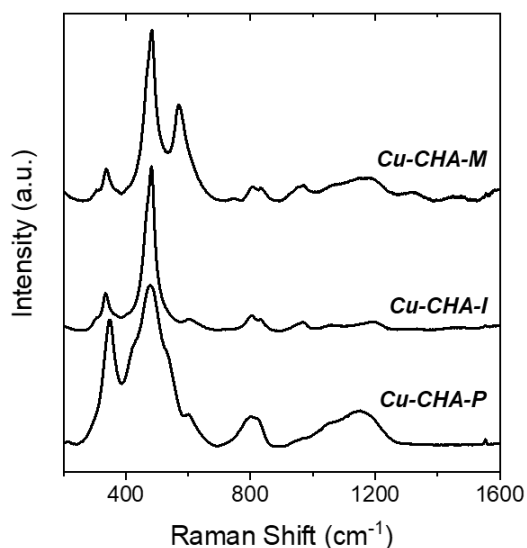### 3.2 Identity of Raman-Active Cu_xO_y Species Formed Over ZCuOH

Figure 2. *In situ* steady-state Raman spectra (λ_{ex} = 532 nm) of Cu-CHA samples containing predominantly Z_2Cu sites (Cu-CHA-P), ZCuOH sites (Cu-CHA-I), or mixtures thereof (Cu-CHA-M) after O_2 activation (21 kPa O_2, 80 kPa He, 723 K). Samples were pretreated in He at 723 K for 2 h prior to the introduction of O_2. All spectra have been normalized to the most-intense feature (~450 cm^{-1}) and are vertically offset for clarity.

The identity of the PMO- and Raman-active Cu_xO_y species must be determined to generate a meaningful model that describes its genesis during O_2 activation. Figure 2 shows steady-state spectra contain several significant vibrational features between 300 – 1,300 cm^{-1}. The sharp features at 330 and 475 cm^{-1} correspond to the $\nu(T-O-T)$ mode of the
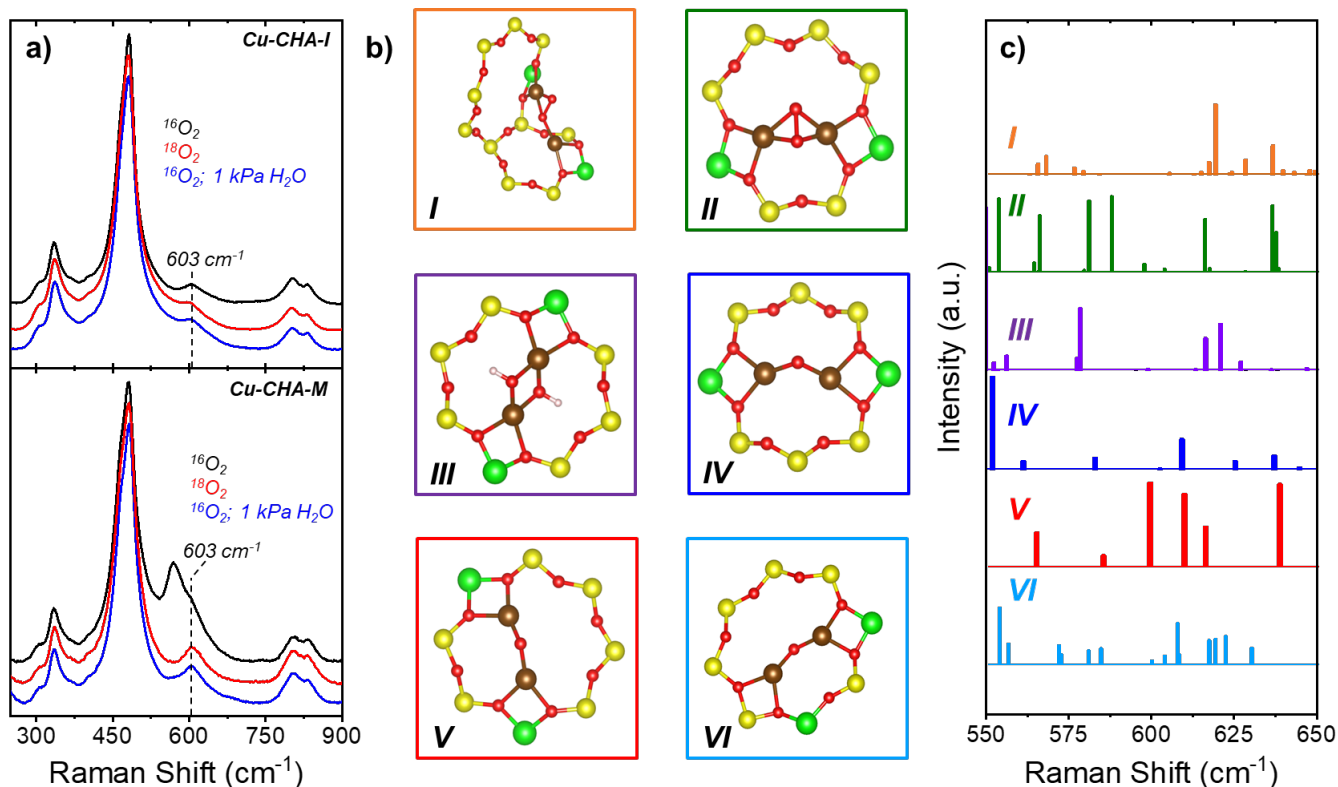
Figure 3. *In situ* steady-state Raman spectra (λ_{ex} = 532 nm) of Cu-CHA-I (top) and Cu-CHA-M (bottom) after O_2 activation (21 kPa O_2, 80 kPa He, 723 K) with natural abundance $^{16}O_2$ (black), $^{18}O_2$ (red), or $^{16}O_2$ with 1 kPa of H_2O (blue). b) Optimized geometries of Cu dimers I (orange, *trans*-peroxo dicopper), II (green, μ-(η^2:η^2)peroxo dicopper), III (purple, bis(μ-hydroxyl) dicopper), IV (blue, mono-μ-oxo dicopper), V (red, mono-μ-oxo dicopper), and VI (teal, mono-μ-oxo dicopper), where dicopper species IV, V, and VI differ in the arrangement of Al atoms within the 8-membered ring. c) The corresponding simulated Raman-active vibrations for each of the Cu dimers and monomers. Colors within panel c) are consistent with the colored boxes for each Cu dimer in b).

six-membered rings and ν_s(T-O-T), respectively.[46-47] The broad features centered around 800 cm^{-1} and 1100 cm^{-1} correspond to ν_s(Si-O) and ν_{as}(Si-O) modes, which are typical of zeolite frameworks.[46-47] The features at 580 (observed only for Cu-CHA-M) and 603 cm^{-1} have previously been assigned as ν(Cu-O) of a *trans*-μ-1,2-peroxo dicopper(II) intermediate and ν(Cu-O) of a mono-(μ-oxo)dicopper(II) species, respectively.[22] Figure 2 also displays a spectrum of Cu-CHA-P, intended as a control material to contain predominantly Z_2Cu sites that have been reported previously to be PMO-inactive[14] and thus, should not form multinuclear Cu_xO_y species during O_2 activation. Figure 2 shows that the Raman spectrum of O_2-activated Cu-CHA-P possesses a spectral lineshape distinct from Cu-CHA-I and Cu-CHA-M, which suggests that Raman-active species that form on Cu-CHA-P is not the same as the PMO-active species formed on the ZCuOH-containing materials. In the presence of H_2O (0.1 – 1 kPa H_2O, 21 kPa O_2, 723 K, Figure 3A), spectra of Cu-CHA-M show attenuation of the large vibrational feature at 580 cm^{-1} such that these spectra closely resemble those of Cu-CHA-I.

The identity of the species observed during O_2 activation by Raman spectroscopy was evinced through a combination of isotopic labeling and computed Raman spectra of plausible chemical species. Isotopic labeling experiments with $^{18}O_2$ were performed by treating Cu-CHA-I and Cu-CHA-M at 723 K in flowing $^{18}O_2$ (21 kPa $^{18}O_2$, 80 kPa He) to identify vibrational shifts to aid in the identification of reactive Cu_xO_y species formed. Both Cu-CHA-I and Cu-CHA-M possess Raman scattering features at 603 cm^{-1} when either $^{18}O_2$ or $^{16}O_2$ is used (Figure 3). Cu-CHA-M activated in O_2 under dry conditions, however, possesses an additional feature around 580 cm^{-1} previously attributed to *trans*-μ-1,2-peroxo dicopper(II).[22] Consequently, these data suggest that the presence of H_2O deliberately added to $^{16}O_2$ or present in trace amounts within $^{18}O_2$ aid in the structural conversion of *trans*-μ-1,2-peroxo dicopper(II) to form the species that exhibits a Raman scattering at 603 cm^{-1}. Notably, these findings differ from those of Lobo and coworkers, who observed an isotopic shift ($\Delta^{18}O_2$) of 24 cm^{-1} for the vibration at 603 cm^{-1}.[22] In their work, a scattering feature at 836 cm^{-1} was assigned to ν(O-O) of *trans*-μ-1,2-peroxo dicopper.[22] Here, the lack of shift in the Raman spectra of $^{18}O_2$-activated Cu-CHA zeolites seems to exclude this possibility. Consequently, the broad features centered around 800 and 1100 cm^{-1} (Figure 2) appear to reflect framework ν_s(Si-O) and ν_{as}(Si-O) modes that are strongly scattered based upon preferential excitation (i.e., resonance) of Cu_xO_y species they stabilize.

To aid in spectral assignments, we used DFT+U to model frequently discussed Cu dimer structures (Figure 3b) and calculate their Raman spectra (Figure 3c).[20] For each
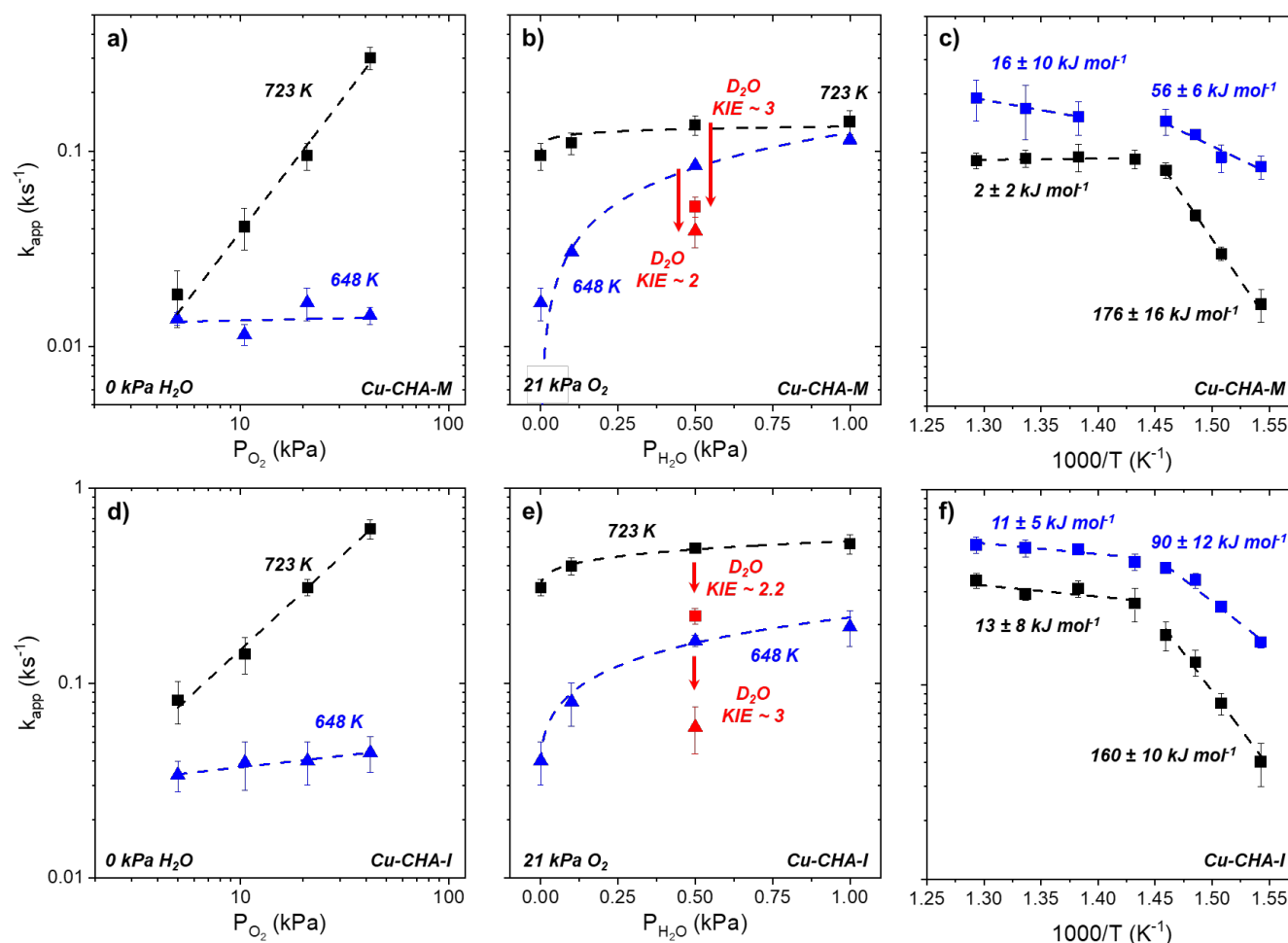

Figure 4. Apparent rate constants (k_{app}) for ZCuOCuZ formation over Cu-CHA-M (panels a, b and c) and Cu-CHA-I (panels d, e, and f) as function of a, d) P_{O_2} (0 kPa H_2O); b, e) P_{H_2O} (21 kPa O_2) at 723 K (■) and 648 K (▲); and c, f) inverse temperature with water vapor (▲, 0.5 kPa H_2O, 21 kPa O_2) or in the absence of water (■, 0 kPa H_2O, 21 kPa O_2). All samples were pretreated (101 kPa He, 723 K, 2 h) prior to introducing O_2. Dashed curves in panels a, b, d, and e represent power-law fits, while those in panels c and f are fits of the Arrhenius equation. Values listed within panels c and f correspond to the apparent activation energies within the different kinetic regimes, obtained through fits of the Arrhenius equation.

optimized structure, the change in polarizability was calculated along the normal modes of the simulated vibrations to determine the frequencies of Raman-active vibrations (see Section 2.4 for full details).[48] The precise assignment of a complex whose calculated molecular vibrations describe the Raman features in Figures 1 and 3a (i.e., at 603 cm^{-1}) requires that several criteria be met. First, the Cu$_x$O$_y$ complex must exist as Cu(II), which excludes the possibility of bis-μ-oxo dicopper and trimeric Cu-oxo complexes.[27, 29] Second, the Cu$_x$O$_y$ intermediate must absorb 532 nm (18,800 cm^{-1}; Figures S3 and S5) light to provide the resonance Raman effect. Third, the candidate dimer structures modeled must possess Raman scattering features within 20 cm^{-1} of the experimentally measured vibrations, which is the range of deviations between experimental and theoretical frequencies commonly reported for similar materials.[49-50] Fourth, the simulated vibration near 603 cm^{-1} must not contain significant Cu-O or O-O bond deformations (e.g., stretching modes

of superoxo or peroxo complexes), as these vibrations would produce a significant $\Delta^{18}O_2$.

Among the complexes depicted in Figure 3b, mono(μ-oxo) dimer species (IV, V, and VI) most closely satisfy these criteria. These complexes exhibit strong absorbance between 8,000 – 20,000 cm^{-1} correspond to d-d transitions.[20] Frequency calculations show that these species also possess a significant Raman scattering features between 590 – 620 cm^{-1} that do not show significant deformation of the Cu-O bonds (Supporting Information, Videos). In comparison, our calculations[20] show that Cu dimers I – III (Figure 3b) do not have significant UV-Vis absorbance features near 18,800 cm^{-1} and do not possess Raman features near 603 cm^{-1} that correspond to vibrations with significant Cu-O or O-O bond deformations (which is inconsistent with $\Delta^{18}O_2$ = 0). Consequently, the Cu$_x$O$_y$ species that form over Cu-CHA-I and Cu-CHA-M over long time scales (0 – 15 ks) are active for PMO and that are responsible for the 603 cm^{-1} feature

likely correspond to mono(μ-oxo)dicopper intermediates. We note, however, that the precise and unambiguous assignment of the 603 cm⁻¹ Raman scattering feature to a multinuclear vibration of mono(μ-oxo)dicopper species remains difficult as DFT+U calculations are performed off-resonance and do not account for the preferential excitation of vibrations due to induced electronic transitions. Consequently, we tentatively assign the species responsible for the observed Raman feature at 603 cm⁻¹ and for PMO reactivity as a mono(μ-oxo)dicopper species but do not exclude any of the plausible isomers (species IV, V, or VI). For brevity, we refer to mono(μ-oxo)dicopper as ZCuOCuZ in the following sections.

3.3 Mechanistic Interpretations of Mean-Field O_2 Activation Kinetics

Observations presented earlier in this report suggest that rates of ZCuOCuZ formation over Cu(I) ions likely depend on O_2 and H_2O pressure with a functional form resembling

$$r_{App} = k_{form} P_{O_2}^a P_{H_2O}^b [Cu(I)] \qquad (3)$$

where k_{form} is the rate constant for ZCuOCuZ formation, P_i is the partial pressure of species i, a and b represent the power-law dependence of rates on P_{O_2} and P_{H_2O}, respectively, and $[Cu(I)]$ is the number of Cu(I) species. The conversions of O_2 and H_2O remain differential (< 1%) throughout the formation of ZCuOCuZ complexes, because these reactants are introduced with molar flowrates that greatly exceed the consumption of Cu(I) ions within the sample over the relevant timescales for ZCuOCuZ formation (1 – 150 ks).[51] As such, the rate of ZCuOCuZ formation can be stated in a form that reflects a pseudo-first-order dependence on [Cu(I)]
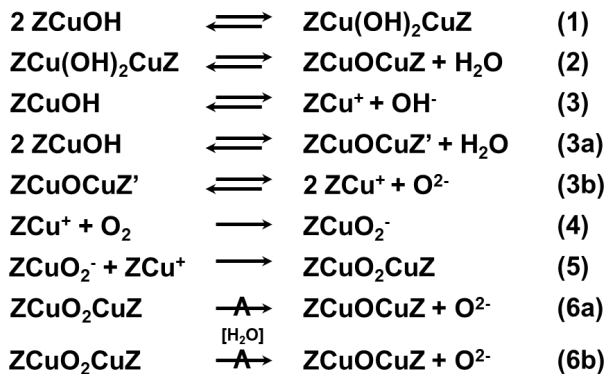
$$r_{App} = k_{app} [Cu(I)] \qquad (4)$$

where k_{app} is the apparent rate constant for ZCuOCuZ formation and implicitly contains the dependence of O_2 activation rates on P_{O_2} and P_{H_2O}.

Figures 4c and 4f show that values of k_{app} over Cu-CHA-I and Cu-CHA-M samples exhibit two distinct kinetic regimes at low (648 – 673 K) and high (685 – 773 K) temperature. The Cu-CHA-P control sample prepared to contain predominantly Z_2Cu sites was omitted from this analysis because this sample does not facilitate PMO. At low temperatures, rates of ZCuOCuZ formation do not depend on P_{O_2}, exhibit saturation kinetics (i.e., a first-to-zeroth order transition) in P_{H_2O}, and increase exponentially with temperature under either dry conditions (E_a = 176 ± 16 kJ mol⁻¹) or with 0.5 kPa H_2O present (E_a = 56 ± 6 kJ mol⁻¹). In contrast, at high temperatures, ZCuOCuZ formation rates depend linearly on P_{O_2}, remain nearly constant at all P_{H_2O}, and present negligible temperature dependence (i.e., are nearly barrierless). Moreover, ZCuOCuZ formation rates exhibit a normal kinetic isotope effect ($k_{app,H}/k_{app,D}$ = 2 – 3.2, 21 kPa O_2, 0.5 kPa H_2O or D_2O) at both 648 and 723 K, which in conjunction with the functional dependence of formation rates on P_{H_2O}, suggests that H_2O participates in the activation of O_2. Comparisons between rate dependences for ZCuOCuZ formation at low (< 673 K) and high (> 685 K) temperatures

suggest that Cu ions are saturated with O_2-derived intermediates at low temperatures, while Cu sites are not occupied by an O_2-derived species at high temperatures. ZCuOCuZ formation rates depend similarly on reactant pressures, temperature, and the isotopologue of water used for both Cu-CHA-I and Cu-CHA-M samples, which strongly suggests that the kinetically competent species probed *via* Raman spectroscopy within these samples are the same (i.e., corresponding to ZCuOCuZ formation from ZCu⁺ species).

Scheme 1. A series of plausible chemical transformations that describe ZCuOH reduction and O_2 activation to form ZCuOCuZ species. Z denotes a framework Al atom. Step 3 represents ZCuOH auto-reduction and is described by two hypothetical steps (steps 3a and 3b). The [H_2O] within step 6 represents the catalytic role of H_2O in O-O bond dissociation. ZCuOCuZ represents the Raman-active intermediate, and a ^ atop an arrow denotes a kinetically-relevant step.

2 ZCuOH	$\rightleftharpoons$	**ZCu(OH)₂CuZ**	**(1)**
ZCu(OH)₂CuZ	$\rightleftharpoons$	**ZCuOCuZ + H₂O**	**(2)**
ZCuOH	$\rightleftharpoons$	**ZCu⁺ + OH⁻**	**(3)**
2 ZCuOH	$\rightleftharpoons$	**ZCuOCuZ' + H₂O**	**(3a)**
ZCuOCuZ'	$\rightleftharpoons$	**2 ZCu⁺ + O²⁻**	**(3b)**
ZCu⁺ + O₂	$\longrightarrow$	**ZCuO₂⁻**	**(4)**
ZCuO₂⁻ + ZCu⁺	$\longrightarrow$	**ZCuO₂CuZ**	**(5)**
ZCuO₂CuZ	$\xrightarrow[\text{[H₂O]}]{\text{^}}$	**ZCuOCuZ + O²⁻**	**(6a)**
ZCuO₂CuZ	$\xrightarrow{\text{^}}$	**ZCuOCuZ + O²⁻**	**(6b)**

Scheme 1 shows a plausible series of chemical transformations that describe the formation of ZCuOCuZ species upon contact between O_2 and Cu(I) ions within Cu-CHA materials. Two ZCuOH moieties react to form a bis(μ-hydroxyl)dicopper species (ZCu(OH)₂CuZ; step 1), which then dehydrates to form ZCuOCuZ species (step 2). Alternatively, treatments in He (or CO, *vide infra*) auto-reduce some fraction of ZCuOH sites to form ZCu⁺ sites (step 3)[14, 20, 44] that subsequently oxidize by chemisorbing molecular O_2 to form ZCuO₂⁻ intermediates (step 4). Reaction between ZCuO₂⁻ and a proximate ZCu⁺ forms a bridging dicopper peroxide complex (ZCuO₂CuZ; step 5).[52] These ZCuO₂CuZ species may be active intermediates for PMO or may undergo O-O bond cleavage in the absence (step 6a) or presence of H_2O (step 6b) to form ZCuOCuZ and release an equivalent of $O²⁻$. These ZCuOCuZ complexes appear to form irreversibly, because the Raman features attributed to this species (580 cm⁻¹) persist for hours under flowing He after activation with O_2, in agreement with previous reports.[22] Considering the processes described by Scheme 1, the rapid oxidation of Cu(I) to Cu(II) observed by XAS (Figure 1d) likely corresponds to step 4 or step 5.

To examine whether auto-reduction (steps 1 – 3, Scheme 1) possibly contributes to the formation of ZCuOCuZ, we investigated the influence of different reductive pretreatments of ZCuOH sites. Auto-reduction treatments of ZCuOH species in He at 723 K do not fully reduce all Cu(II) complexes present to Cu(I) (Figure 1).[14, 20, 22] Rather, treatments in He yield a combination of ZCu⁺, ZCuₓOᵧHᵤ, and Z₂Cu species that do not auto-reduce. The Raman active ZCuOCuZ

species seem unlikely to form via the dehydration of ZCu(OH)$_2$CuZ (step 2, Scheme 1), because no Raman features appear at elevated temperatures in He (Figure 1a). We also used Raman spectrokinetics to measure rates of ZCuOCuZ formation over Cu-CHA-I samples treated in carbon monoxide (5 kPa CO, 96 kPa He, 523 K), which fully reduces multinuclear Cu$_x$O$_y$ sites to ZCu$^+$.[20] Following these CO pretreatments, we observe ZCuOCuZ formation rates that depend on O$_2$ pressure, temperature, and D$_2$O/H$_2$O (Section S8) similarly as Cu-CHA-I instead auto-reduced in He. These comparisons demonstrate that step 1 and step 2 are not kinetically relevant for the formation of the ZCuOCuZ complex after a He auto-reduction treatment. Finally, we must note that this sequence of reactions (steps 1 – 3, Scheme 1) does not involve gaseous O$_2$; therefore, these steps do not explain the dependence of ZCuOCuZ formation rates on the pressure of O$_2$ (Figs 4a and 4d). Consequently, the subsequent and slower formation of the Raman active ZCuOCuZ complexes must reflect steps 6a or 6b if O-O bond rupture limits rates.

To test if our series of hypothetical steps can account for the observed rates of ZCuOCuZ formation, we derive a simple rate expression based on steps 4 – 6 in Scheme 1. In this model, the rate of ZCuOCuZ formation is given by

$$\frac{d[ZCuOCuZ]}{dt} = k_6[ZCuO_2CuZ] \tag{5}$$

where k_i represents the rate constant for step i, and $[a]$ represents either the number of a given species (i.e., if it is a surface species, such as ZCuOCuZ) or the activity of the gas-phase species (e.g., O$_2$). Under these reaction conditions (i.e., low pressures and high temperatures), the activities are equal to the partial pressure. Step 6b implies that ZCuOCuZ formation involves H$_2$O, which we rationalize as either solvation of the transition state for the O-O bond rupture or evidence that proton transfer facilitates this event. Invoking the pseudo-steady state assumption on $[ZCuO_2CuZ]$ and $[ZCuO_2^-]$ species simplifies equation 5 to yield

$$\frac{d[ZCuOCuZ]}{dt} = k_4[ZCu^+][O_2] \tag{6}$$

The expression for $[ZCu^+]$ arises from a site balance over all likely surface intermediates present in steps 4, 5, and 6

$$[L] = [ZCu^+] + [ZCuO_2^-] + [ZCuO_2CuZ] \tag{7}$$

$$[L] = [ZCu^+]\left(1 + \frac{k_4}{k_5}[O_2] + \frac{k_5}{k_6}[O_2][ZCu^+]\right) \tag{8}$$

where $[L]$ represents the total number of Cu ions that form Raman-active intermediates and the three terms within the parentheses of equation 8 correspond to the relative coverages of ZCu$^+$, ZCuO$_2^-$, and ZCuO$_2$CuZ species, respectively. Substitution of equation 8 into equation 6 yields

$$\frac{d[ZCuOCuZ]}{dt}\frac{1}{[L]} = \frac{k_4[O_2]}{\left(1 + \frac{k_4}{k_5}[O_2] + \frac{k_5}{k_6}[O_2][ZCu^+]\right)} \tag{9}$$

At low temperatures, the chemisorption of O$_2$ is facile, which suggests that an O$_2$-derived intermediate (e.g., ZCuO$_2^-$

) comprises the most-abundant reactive intermediate (MARI). Equation 9 collapses to a simpler form with this approximation

$$\frac{d[ZCuOCuZ]}{dt}\frac{1}{[L]} = k_5 \tag{10}$$

In contrast, the entropic losses incurred by O$_2$ chemisorption prevail at higher temperatures, which leads to ZCu$^+$ as the MARI and reduces equation 9 to

$$\frac{d[ZCuOCuZ]}{dt}\frac{1}{[L]} = k_4[O_2] \tag{11}$$

Equations 10 and 11 quantitatively describe the O$_2$ dependence on the rates of ZCuOCuZ formation, while the complex and likely non-elementary role of water molecules is captured within k_6 (Scheme 1).

While Scheme 1 and equations 5 – 9 yield functional expressions that describe O$_2$ activation kinetics, we note that this series of chemical transformations arises largely from chemical intuition and experimental observations. The unambiguous identification of the elementary steps that lead to ZCuOCuZ formation requires a combination of currently inaccessible synthetic methods and DFT-calculated reaction trajectories. Furthermore, DFT-calculated reaction pathways to quantitatively evaluate the free energy landscape of O$_2$ activation may not yield meaningful results to interpret experimental data, because the values calculated are a strong function of the Al arrangement that influences the binuclear Cu configurations chosen. Even nominally "single-site" Cu-CHA samples that contain only 6-MR isolated Al sites possess multiple types of Al-Al pair configurations in 8-MR windows that influence the energetics of binuclear Cu-oxo species formed.

Collectively, these results present evidence for the involvement of the ZCuOCuZ complex as an active intermediate for PMO and a plausible series of chemical steps for O$_2$ activation over ZCuOH sites consistent with the observed dependence of O$_2$ activation on O$_2$ and H$_2$O pressure, protons, and temperature. The precise identification of binuclear Cu species responsible for a specific chemistry (e.g., NO decomposition, CH$_3$OH synthesis), however, remains an important scientific challenge.

4.0 CONCLUSIONS
Cu-ion exchanged CHA zeolites that contain detectable quantities of ZCuOH activate molecular O$_2$ to form Cu$_x$O$_y$ species active for partial methane oxidation (PMO), nitrogen oxide decomposition, and carbon monoxide oxidation. Temporally-resolved resonance Raman spectroscopy (λ_{ex} = 532 nm) evinces the genesis of reactive Cu$_x$O$_y$ species that form at ZCuOH sites via the activation of O$_2$. The population of these Raman-active species correlate strongly with increases in the yield of methanol from stoichiometric PMO, whereas, rates of the bulk oxidation of Cu(I) to Cu(II) proceed significantly faster as observed with X-ray absorption spectroscopy. These kinetic comparisons suggest that kinetically-relevant structural rearrangements (and O-O bond rupture) determine formation rates of the Cu$_x$O$_y$ complex responsible for methanol formation and that rates of Cu(I) oxidation do not correspond to the formation of the reactive intermediate.

The Raman active Cu_xO_y complex possesses a distinct vibrational feature at 603 cm^{-1} assigned to the deformational mode of the 8-membered ring of a mono(μ-oxo)dicopper intermediate (ZCuOCuZ), through comparisons of measured spectra with Raman scattering frequencies calculated via density functional theory. The rates of O_2 activation of ZCuOH-containing CHA samples show two distinct kinetic regimes at low (< 673 K) and high (> 685 K) temperatures. At low temperatures, rates of O_2 activation do not depend on O_2 pressure, show a first-to-zeroth order kinetic dependence on H_2O pressure, and exhibit a normal H_2O/D_2O KIE. At high temperatures, O_2 activation rates increase linearly with O_2 pressure, show a weak dependence on H_2O pressure, and possess a normal KIE on H_2O/D_2O. These observations agree with a plausible mechanism in which a fraction of ZCuOH sites initially reduce to form ZCu^+ sites and readily bind molecular O_2 to form $ZCuO_2$ intermediates. ZCu^+ and $ZCuO_2$ then react to form a $ZCuO_2CuZ$ complex. These $ZCuO_2CuZ$ intermediates undergo kinetically relevant O-O bond scission, which can be facilitated by water, to form ZCuOCuZ species and O^{2-}.

These data, methodologies, and interpretation provide a basis to understand how Cu ions within zeolites activate O_2 and evolve to form species responsible for socially- and environmentally-important oxidation chemistries. The precise identification of the *active* species and the development of design principles that increase rates and selectivities remains a challenge. These goals motivate the development of synthetic methods to prepare model Cu-zeolites with more uniform Cu structures, innovative kinetic and spectroscopic tools to probe active Cu structures, and connections between experimental data and computational models to understand these complex systems.

ASSOCIATED CONTENT

Supporting Information. CHA synthesis methods, Cu ion exchange, UV-vis spectroscopy, Cu-CHA characterization, *in situ* X-ray absorption spectroscopy, methanol yields, simulated Raman spectra, *in situ* Raman spectrokinetics on CO-reduced Cu-CHA-I

AUTHOR INFORMATION

Corresponding Author

*dwflhrty@illinois.edu

Author Contributions

The manuscript was written through contributions of all authors. All authors have given approval to the final version of the manuscript.

ACKNOWLEDGMENT

REFERENCES

1. Groothaert, M. H.; Van Bokhoven, J. A.; Battiston, A. A.; Weckhuysen, B. M.; Schoonheydt, R. A., Bis(μ-oxo)dicopper in Cu-ZSM-5 and Its Role in the Decomposition of NO: A Combined in Situ XAFS, UV-Vis-Near-IR, and Kinetic Study. *J. Am. Chem. Soc.* **2003**, *125*, 7629-7640.

2. Da Costa, P.; Modén, B.; Meitzner, G. D.; Lee, D. K.; Iglesia, E., Spectroscopic and chemical characterization of active and inactive Cu species in NO decomposition catalysts based on Cu-ZSM5. *Phys. Chem. Chem. Phys.* **2002**, *4*, 4590-4601.

3. Sengupta, D.; Schneider, W. F.; Hass, K. C.; Adams, J. B., CO oxidation catalyzed by Cu-exchanged zeolites: a density functional theory study. *Catal. Lett.* **1999**, *61*, 179-186.

4. Matsumoto, H.; Tanabe, S., Catalytic Behavior and Structure of Active Species of Cu-Y Zeolite in Oxidation of Carbon Monoxide. *J. Phys. Chem.* **1990**, *94*, 4207-4212.

5. Jones, C. B.; Khurana, I.; Krishna, S. H.; Shih, A. J.; Delgass, W. N.; Miller, J. T.; Ribeiro, F. H.; Schneider, W. F.; Gounder, R., Effects of dioxygen pressure on rates of NO_x selective catalytic reduction with NH_3 on Cu-CHA zeolites. *J. Catal.* **2020**, *389*, 140-149.

6. Paolucci, C.; Khurana, I.; Parekh, A. A.; Li, S.; Shih, A. J.; Li, H.; Di Iorio, J. R.; Albarracin Caballero, J. D.; Yezerets, A.; Miller, J. T.; Delgass, N. W.; Ribeiro, F. H.; Schneider, W. F.; Gounder, R., Dynamic multinuclear sites formed by mobilized copper ions in NO_x selective catalytic reduction. *Science* **2017**, *357*, 898-903.

7. Paolucci, C.; Parekh, A. A.; Khurana, I.; Di Iorio, J. R.; Li, H.; Albarracin Caballero, J. D.; Shih, A. J.; Anggara, T.; Delgass, W. N.; Miller, J. T.; Ribeiro, F. H.; Gounder, R.; Schneider, W. F., Catalysis in a Cage: Condition-Dependent Speciation and Dynamics of Exchanged Cu Cations in SSZ-13 Zeolites. *J. Am. Chem. Soc.* **2016**, *138* (18), 6028-6048.

8. Shih, A. J.; Khurana, I.; Li, H.; González, J.; Kumar, A.; Paolucci, C.; Lardinois, T. M.; Jones, C. B.; Albarracin Caballero, J. D.; Kamasamudram, K.; Yezerets, A.; Delgass, W. N.; Miller, J. T.; Villa, A. L.; Schneider, W. F.; Gounder, R.; Ribeiro, F. H., Spectroscopic and kinetic responses of Cu-SSZ-13 to SO_2 exposure and implications for NO_x selective catalytic reduction. *Appl. Catal. A* **2019**, *574*, 122-131.

9. Krishna, S. H.; Jones, C. B.; Miller, J. T.; Ribeiro, F. H.; Gounder, R., Combining Kinetics and Operando Spectroscopy to Interrogate the Mechanism and Active Site Requirements of NOx Selective Catalytic Reduction with NH_3 on Cu-Zeolites. *J Phys. Chem. Lett.* **2020**, *11* (13), 5029-5036.

10. Groothaert, M. H.; Smeets, P. J.; Sels, B.; Jacobs, P. A.; Schoonheydt, R. A., Selective Oxidation of Methane by the Bis(μ-oxo)dicopper Core Stabilized on ZSM-5 and Mordenite Zeolites. *J. Am. Chem. Soc.* **2005**, *127*, 1394-1395.

11. Woertink, J. S.; Smeets, P. J.; Groothaert, M. H.; Vance, M. A.; Sels, B. F.; Schoonheydt, R. A.; Solomon, E. I., A $[Cu_2O]^{2+}$ core in Cu-ZSM-5, the active site in the oxidation of methane to

methanol. *Proc. Natl. Acad. Sci.* **2009,** *106* (45), 18908-18913.

12. Dinh, K. T.; Sullivan, M. M.; Serna, P.; Meyer, R. J.; Dincǎ, M.; Román-Leshkov, Y., Viewpoint on the Partial Oxidation of Methane to Methanol Using Cu- and Fe-Exchanged Zeolites. *ACS Catal.* **2018,** *8* (9), 8306-8313.

13. Pappas, D. K.; Martini, A.; Dyballa, M.; Kvande, K.; Teketel, S.; Lomachenko, K. A.; Baran, R.; Glatzel, P.; Arstad, B.; Berlier, G.; Lamberti, C.; Bordiga, S.; Olsbye, U.; Svelle, S.; Beato, P.; Borfecchia, E., The Nuclearity of the Active Site for Methane to Methanol Conversion in Cu-Mordenite: A Quantitative Assessment. *J. Am. Chem. Soc.* **2018,** *140* (45), 15270-15278.

14. Pappas, D. K.; Borfecchia, E.; Dyballa, M.; Pankin, I. A.; Lomachenko, K. A.; Martini, A.; Signorile, M.; Teketel, S.; Arstad, B.; Berlier, G.; Lamberti, C.; Bordiga, S.; Olsbye, U.; Lillerud, K. P.; Svelle, S.; Beato, P., Methane to Methanol: Structure-Activity Relationships for Cu-CHA. *J. Am. Chem. Soc.* **2017,** *139* (42), 14961-14975.

15. Borfecchia, E.; Pappas, D. K.; Dyballa, M.; Lomachenko, K. A.; Negri, C.; Signorile, M.; Berlier, G., Evolution of active sites during selective oxidation of methane to methanol over Cu-CHA and Cu-MOR zeolites as monitored by operando XAS. *Catal. Today* **2019,** *333*, 17-27.

16. Alayon, E. M.; Nachtegaal, M.; Bodi, A.; Ranocchiari, M.; van Bokhoven, J. A., Bis(mu-oxo) versus mono(mu-oxo)dicopper cores in a zeolite for converting methane to methanol: an in situ XAS and DFT investigation. *Phys. Chem. Chem. Phys.* **2015,** *17* (12), 7681-93.

17. Brezicki, G.; Kammert, J. D.; Gunnoe, T. B.; Paolucci, C.; Davis, R. J., Insights into the Speciation of Cu in the Cu-H-Mordenite Catalyst for the Oxidation of Methane to Methanol. *ACS Catal.* **2019,** *9* (6), 5308-5319.

18. Dinh, K. T.; Sullivan, M. M.; Narsimhan, K.; Serna, P.; Meyer, R. J.; Dinca, M.; Roman-Leshkov, Y., Continuous Partial Oxidation of Methane to Methanol Catalyzed by Diffusion-Paired Copper Dimers in Copper-Exchanged Zeolites. *J. Am. Chem. Soc.* **2019,** *141* (29), 11641-11650.

19. Narsimhan, K.; Iyoki, K.; Dinh, K.; Roman-Leshkov, Y., Catalytic Oxidation of Methane into Methanol over Copper-Exchanged Zeolites with Oxygen at Low Temperature. *ACS Cent Sci* **2016,** *2* (6), 424-429.

20. Li, H.; Paolucci, C.; Khurana, I.; Wilcox, L. N.; Goltl, F.; Albarracin-Caballero, J. D.; Shih, A. J.; Ribeiro, F. H.; Gounder, R.; Schneider, W. F., Consequences of exchange-site heterogeneity and dynamics on the UV-visible spectrum of Cu-exchanged SSZ-13. *Chem Sci* **2019,** *10* (8), 2373-2384.

21. Tomkins, P.; Ranocchiari, M.; van Bokhoven, J. A., Direct Conversion of Methane to Methanol under Mild Conditions over Cu-Zeolites and beyond. *Acc. Chem. Res.* **2017,** *50* (2), 418-425.

22. Ipek, B.; Wulfers, M. J.; Kim, H.; Göltl, F.; Hermans, I.; Smith, J. P.; Booksh, K. S.; Brown, C. M.; Lobo, R. F., Formation of $[Cu_2O_2]^{2+}$ and $[Cu_2O]^{2+}$ toward C–H Bond Activation in Cu-SSZ-13 and Cu-SSZ-39. *ACS Catal.* **2017,** *7* (7), 4291-4303.

23. Vanelderen, P.; Hadt, R. G.; Smeets, P. J.; Solomon, E. I.; Schoonheydt, R. A.; Sels, B. F., Cu-ZSM-5: A biomimetic inorganic model for methane oxidation. *J. Catal.* **2011,** *284* (2), 157-164.

24. Vanelderen, P.; Snyder, B. E.; Tsai, M. L.; Hadt, R. G.; Vancauwenbergh, J.; Coussens, O.; Schoonheydt, R. A.; Sels, B. F.; Solomon, E. I., Spectroscopic definition of the copper active sites in mordenite: selective methane oxidation. *J. Am. Chem. Soc.* **2015,** *137* (19), 6383-6392.

25. Nachtigall, P.; Arean, C. O., Themed Issue on characterization of adsorbed species. *Phys. Chem. Chem. Phys.* **2010,** *12* (24), 6307-6308.

26. Knorpp, A.; Pinar, A. B.; Baerlocher, C.; McCusker, L. B.; Casati, N.; Newton, M. A.; Checchia, S.; Meyet, J.; Palagin, D.; van Bokhoven, J. A., Paired copper monomers in zeolite omega: the active site for methane-to-methanol conversion. *Angew. Chem. Int. Ed.* **2020,** *60*, 1-6.

27. Grundner, S.; Markovits, M. A.; Li, G.; Tromp, M.; Pidko, E. A.; Hensen, E. J.; Jentys, A.; Sanchez-Sanchez, M.; Lercher, J. A., Single-site trinuclear copper oxygen clusters in mordenite

for selective conversion of methane to methanol. *Nat Commun.* **2015,** *6*, 7546.

28. Li, G.; Vassilev, P.; Sanchez-Sanchez, M.; Lercher, J. A.; Hensen, E. J. M.; Pidko, E. A., Stability and reactivity of copper oxo-clusters in ZSM-5 zeolite for selective methane oxidation to methanol. *J. Catal.* **2016,** *338*, 305-312.

29. Grundner, S.; Luo, W.; Sanchez-Sanchez, M.; Lercher, J. A., Synthesis of single-site copper catalysts for methane partial oxidation. *Chem. Commun.* **2016,** *52* (12), 2553-2556.

30. Newton, M. A.; Knorpp, A. J.; Sushkevich, V. L.; Palagin, D.; van Bokhoven, J. A., Active sites and mechanisms in the direct conversion of methane to methanol using Cu in zeolitic hosts: a critical examination. *Chem. Soc. Rev.* **2020,** *49* (5), 1449-1486.

31. Sushkevich, V. L.; Palagin, D.; van Bokhoven, J. A., The Effect of the Active-Site Structure on the Activity of Copper Mordenite in the Aerobic and Anaerobic Conversion of Methane into Methanol. *Angew. Chem. Int. Ed. Engl.* **2018,** *57* (29), 8906-8910.

32. Borfecchia, E.; Beato, P.; Svelle, S.; Olsbye, U.; Lamberti, C.; Bordiga, S., Cu-CHA - a model system for applied selective redox catalysis. *Chem. Soc. Rev.* **2018,** *47* (22), 8097-8133.

33. Di Iorio, J. R.; Gounder, R., Controlling the Isolation and Pairing of Aluminum in Chabazite Zeolites Using Mixtures of Organic and Inorganic Structure-Directing Agents. *Chem. Mater.* **2016,** *28* (7), 2236-2247.

34. Devos, J.; Bols, M. L.; Plessers, D.; Goethem, C. V.; Seo, J. W.; Hwang, S.-J.; Sels, B. F.; Dusselier, M., Synthesis–Structure–Activity Relations in Fe-CHA for C–H Activation: Control of Al Distribution by Interzeolite Conversion. *Chem. Mater.* **2019,** *32* (1), 273-285.

35. Koishybay, A.; Shantz, D. F., Water Is the Oxygen Source for Methanol Produced in Partial Oxidation of Methane in a Flow Reactor over Cu-SSZ-13. *J. Am. Chem. Soc.* **2020,** *142,* 11962-11966.

36. Sushkevich, V. L.; Palagin, D.; Ranocchiari, M.; Van Bokhoven, J. A., Selective anaerobic oxidation of methane enables direct synthesis of methanol. *Science* **2017,** *356*, 523-527.

37. Witzke, M. E.; Almithn, A.; Coonrod, C. L.; Triezenberg, M. D.; Hibbitts, D. D.; Flaherty, D. W., In Situ Methods for Identifying Reactive Surface Intermediates during Hydrogenolysis Reactions: C–O Bond Cleavage on Nanoparticles of Nickel and Nickel Phosphides. *J. Am. Chem. Soc.* **2019,** *141*, 16671-16684.

38. Kresse, G.; Furthmüller, J., Efficient iterative schemes for ab initio total-energy calculations using a plane-wave basis set. *Phys. Rev. B* **1996,** *54*, 11169-11184.

39. Grimme, S.; Antony, J.; Ehrlich, S.; Krieg, H., A consistent and accurate ab initio parametrization of density functional dispersion correction (DFT-D) for the 94 elements H-Pu. *J. Chem. Phys.* **2010,** *132* (15), 154104.

40. Grimme, S.; Ehrlich, S.; Goerigk, L., Effect of the damping function in dispersion corrected density functional theory. *J. Comput. Chem.* **2011,** *32* (7), 1456-1465.

41. Blöchl, P. E., Projector augmented-wave method. *Phys. Rev. B* **1994,** *50* (24), 17953-17979.

42. Chen, L.; Janssens, T. V. W.; Gronbeck, H., A comparative test of different density functionals for calculations of NH_3-SCR over Cu-Chabazite. *Phys. Chem. Chem. Phys.* **2019,** *21* (21), 10923-10930.

43. Liang, Q.; Dwaraknath, S.; Persson, K. A., High-throughput computation and evaluation of raman spectra. *Sci. Data* **2019,** *6* (1), 135.

44. Sushkevich, V. L.; van Bokhoven, J. A., Revisiting copper reduction in zeolites: the impact of autoreduction and sample synthesis procedure. *Chem. Commun.* **2018,** *54* (54), 7447-7450.

45. Garrido, M.; Rius, F. X.; Larrechi, M. S., Multivariate curve resolution-alternating least squares (MCR-ALS) applied to spectroscopic data from monitoring chemical reactions processes. *Anal Bioanal Chem* **2008,** *390* (8), 2059-2066.

46. Wu, L.; Degirmenci, V.; Magusin, P. C. M. M.; Lousberg, N. J. H. G. M.; Hensen, E. J. M., Mesoporous SSZ-13 zeolite prepared

by a dual-template method with improved performance in the methanol-to-olefins reaction. *J. Catal.* **2013,** *298*, 27-40.

47. Dutta, P. K.; Puri, M., Synthesis and Structure of Zeolite ZSM-5: A Raman Spectroscopic Study. *J. Phys. Chem.* **1987,** *91*, 4329-4333.

48. Zones, S. I., Conversion of Faujasites to High-Silica Chabazite SSZ-13 in the Presence of NNN-Trimethyl-1-adamantammonium Iodide. *J. Chem. Soc., Faraday Trans.* **1991,** *87*, 3709-3716.

49. Fischer, M.; Delgado, M. R.; Areán, C. O.; Duran, C. O., CO adsorption complexes in zeolites: How does the inclusion of dispersion interactions affect predictions made from DFT calculations? The case of Na-CHA. *Theor. Chem. Acc.* **2015,** *134:91*.

50. Zhang, R.; McEwen, J.-S.; Kollár, M.; Gao, F.; Wang, Y.; Szanyi, J.; Peden, C. H. F., NO Chemisorption on Cu/SSZ-13: A Comparative Study from Infrared Spectroscopy and DFT Calculations. *ACS Catal.* **2014,** *4* (11), 4093-4105.

51. For example, over the course of 1 ks, the molar ratio of dioxygen to total Cu within the sample is >5,000.

52. Step 5 is assumed to be irreversible because the heterolytic cleavage of $ZCuO_2CuZ$ to form $ZCuO_2^-$ and ZCu^+ is energetically disfavored.

Table of Contents